

# Staircase Cascaded Fusion of Lightweight Local Pattern Recognition and Long-Range Dependencies for Structural Crack Segmentation

Hui Liu, Chen Jia, Fan Shi, *Member, IEEE*, Xu Cheng, *Member, IEEE*, Mianzhao Wang, and Shengyong Chen *Senior Member, IEEE*

**Abstract**—Detecting cracks with pixel-level precision for key structures is a significant challenge, as existing methods struggle to effectively integrate local textures and pixel dependencies of cracks. Furthermore, these methods often possess numerous parameters and substantial computational requirements, complicating deployment on edge devices. In this paper, we propose a staircase cascaded fusion crack segmentation network (CrackSCF) that generates high-quality crack segmentation maps using minimal computational resources. We constructed a staircase cascaded fusion module that effectively captures local patterns of cracks and long-range dependencies of pixels, and it can suppress background noise well. To reduce the computational resources required by the model, we introduced a lightweight convolution block, which replaces all convolution operations in the network, significantly reducing the required computation and parameters without affecting the network’s performance. To evaluate our method, we created a challenging benchmark dataset called TUT and conducted experiments on this dataset and five other public datasets. The experimental results indicate that our method offers significant advantages over existing methods, especially in handling background noise interference and detailed crack segmentation. The F1 and mIoU scores on the TUT dataset are 0.8382 and 0.8473, respectively, achieving state-of-the-art (SOTA) performance while requiring the least computational resources. The code and dataset is available at <https://github.com/Karl1109/CrackSCF>.

**Index Terms**—Structural cracks segmentation, lightweight networks, cascaded fusion, local patterns, long-range dependencies

## I. INTRODUCTION

**C**RACKS are common defects in structures such as pavements and buildings, which can lead to serious safety issues. Therefore, regular automated inspections are crucial to ensuring production safety [1, 2]. Early automated detection methods used traditional image processing techniques for crack extraction [3–5]. While these methods are easy to implement, their performance in complex scenarios still needs improvement.

This work was supported by National Natural Science Foundation of China (NSFC) (62272342, 62020106004), and Tianjin Natural Science Foundation (23JCJC00070). (Corresponding authors: *Chen Jia, Fan Shi*)

H. Liu, C. Jia, F. Shi, X. Cheng, M. Z. Wang, S. Y. Chen are with the Engineering Research Center of Learning-Based Intelligent System (Ministry of Education), Key Laboratory of Computer Vision and System (Ministry of Education), and School of Computer Science and Engineering, Tianjin University of Technology, Tianjin, 300384, China (e-mail: liuhui1109@stud.tjut.edu.cn, jiachen@email.tjut.edu.cn, shifan@email.tjut.edu.cn, xu.cheng@ieee.org, wzmz@stud.tjut.edu.cn, sy@ieee.org)

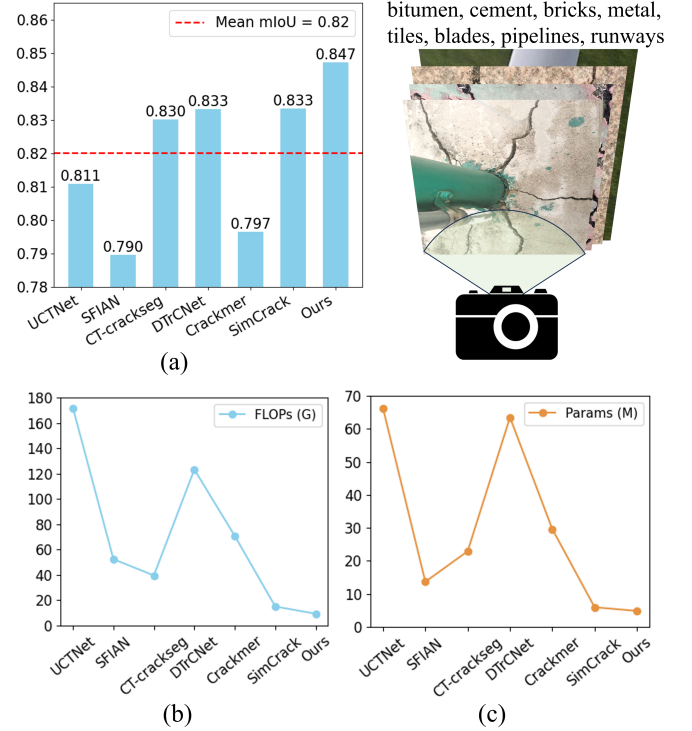


Fig. 1. Performance comparison of our proposed method with UCTNet [6], SFIAN [7], CT-crackseg [8], DTrCNet [9], Crackmer [10] and Simcrack [11] on the TUT dataset in terms of mIoUs, FLOPs and Params metrics.

In recent years, benefiting from the strong local inductive capability of Convolutional Neural Networks (CNN), CNN-based networks such as MST-Net [12] and FcaHRNet [13] have shown efficient feature extraction capabilities in structural crack segmentation tasks. The spatial invariance of CNNs allows them to detect cracks anywhere in an image by learning similar features at different locations. In labeled images, crack labels are long, narrow structures of white pixels, while the background is large black areas. This challenges the model to distinguish between thin cracks and the background. Nevertheless, networks based on CNNs face challenges in capturing long-range dependencies between crack pixels, leading to segmentation discontinuities.

The success of VIT [14] and Swin Transformer [15] has demonstrated the advantages of Transformer [16], with their strong sequence processing capabilities, in handling visual

tasks. Unlike CNNs, transformers can capture dependencies between any pixels when processing images, making them more advantageous in handling complex topologies. To harness the advantages of both CNNs and transformers effectively, researchers have proposed networks such as CATransUNet [17], MFAFNet [18], and Crackmer [9], which integrate local texture information and long-range pixel dependencies through U-shaped connections or residual connections.

Despite the aforementioned methods combining CNN and Transformer have improved performance in pixel-level crack segmentation tasks, they still have some limitations, as follows:

- 1) The different information fusion strategies significantly affect the segmentation performance of CNN-Transformer networks. For instance, UCTNet [6] and CT-crackseg [8] use channel concatenation to fuse local patterns and long-range dependences information. However, concatenation merely stacks the feature information together without deeper feature interaction, failing to understand their correlation and complementarity, resulting in poor segmentation performance on fine cracks and susceptibility to background noise. Additionally, DTrCNet [9] and Crackmer [10] use channel attention to fuse information, which can enhance focus on certain features but neglects spatial information and pixel details in the feature maps, impacting the model's overall performance. As shown in Fig. 1(a), due to these shortcomings, these four methods fail to achieve the best performance.
- 2) Most networks, in pursuit of performance, overlook the significant parameter and computational costs brought by numerous convolution operations. As shown in Fig. 1(b) and Fig. 1(c), networks like SFIAN [7], Crackmer [10], and CT-crackseg[8] have very high computational FLOPs and parameter counts, indicating that they are difficult to implement on resource-limited devices like smartphones and drones, significantly diminishing their practicality.

To address these issues, we propose a staircase cascaded fusion network that can generate high-quality segmentation maps with minimal computational resources while effectively suppressing background noise. Specifically, to better exploit the complementarity and correlation of feature maps without missing critical detail information, we introduce a staircase cascaded fusion module. This module utilizes the pixel attention mechanism, which finely captures local and long-range information, and the channel concatenation mechanism, which progressively integrates features from adjacent layers, to generate crack segmentation maps that comprehensively combine local texture information and pixel dependencies. Furthermore, to decrease the parameter count and computational burden, we introduce a lightweight convolution block called LRDS. This block initially increases and then reduces the channel count, and separates the spatial and channel aspects, thereby minimizing computational costs while maintaining performance.

To assess the structural crack segmentation performance of the model in various complex environments, we also collected a dataset named TUT, which contains 1408 RGB images. Ex-

isting public datasets like DeepCrack [19] and Crack500 [20] include only 1-2 types of scenarios and have relatively simple crack shapes, which are insufficient for thoroughly testing the network's performance. The TUT dataset includes a broader range of real structural crack image scenarios, covering plastic runways, bricks, tiles, cement, bitumen, generator blades, metal materials, and underground pipelines. With such a diverse set of image scenarios, this dataset effectively assesses the network's generalization and robustness. Furthermore, the images feature occlusions, highly complex backgrounds, and uneven lighting, which further enhances the datasets diversity.

In conclusion, our main contributions are as follows:

- 1) We proposed a novel CrackSCF network for structural crack segmentation. By introducing a staircase cascaded fusion module and a lightweight convolution block, this network effectively distinguishes between background and crack pixels with minimal computational resources, resulting in high-quality segmentation maps.
- 2) We collected the TUT dataset, which includes structural cracks in eight different scenarios, providing a more comprehensive evaluation of the network's performance.
- 3) We carried out comprehensive experiments on five public datasets and the TUT benchmark dataset, demonstrating that our proposed CrackSCF network outperforms existing SOTA methods.

The organization of the subsequent sections of this paper is as follows: In Section II, existing crack detection models and lightweight networks are reviewed. Section III details the components of the proposed network. Section IV delves into the experimental details and results. Finally, Section V provides a summary of the entire paper and highlights future research directions.

## II. RELATED WORK

### A. Crack Segmentation Networks

Recently, a growing number of researchers have utilized CNNs to develop crack segmentation networks, achieving advanced performance. Al-Huda et al. [21] proposed the MDAUNet network, based on U-Net and dual attention modules, and designed a hybrid weighted segmentation loss function to address class imbalance issues. Cheng et al. [7] introduced the Selective Feature Fusion and Irregular-Aware Network (SFIAN) to effectively model irregular crack objects, resulting in clearer backgrounds on various crack images. Huang et al. [22] developed a crack detection network for masonry structures that combines thermal imaging and visible light image fusion with semantic segmentation, laying the foundation for the development of cross-modal methods for structural crack monitoring.

Although the aforementioned methods have demonstrated the advantages of CNNs in crack segmentation tasks, CNNs are essentially local operations and cannot effectively perceive a small number of crack pixels amidst a large background. Therefore, these methods often result in discontinuous crack pixels and are highly susceptible to background noise interference.

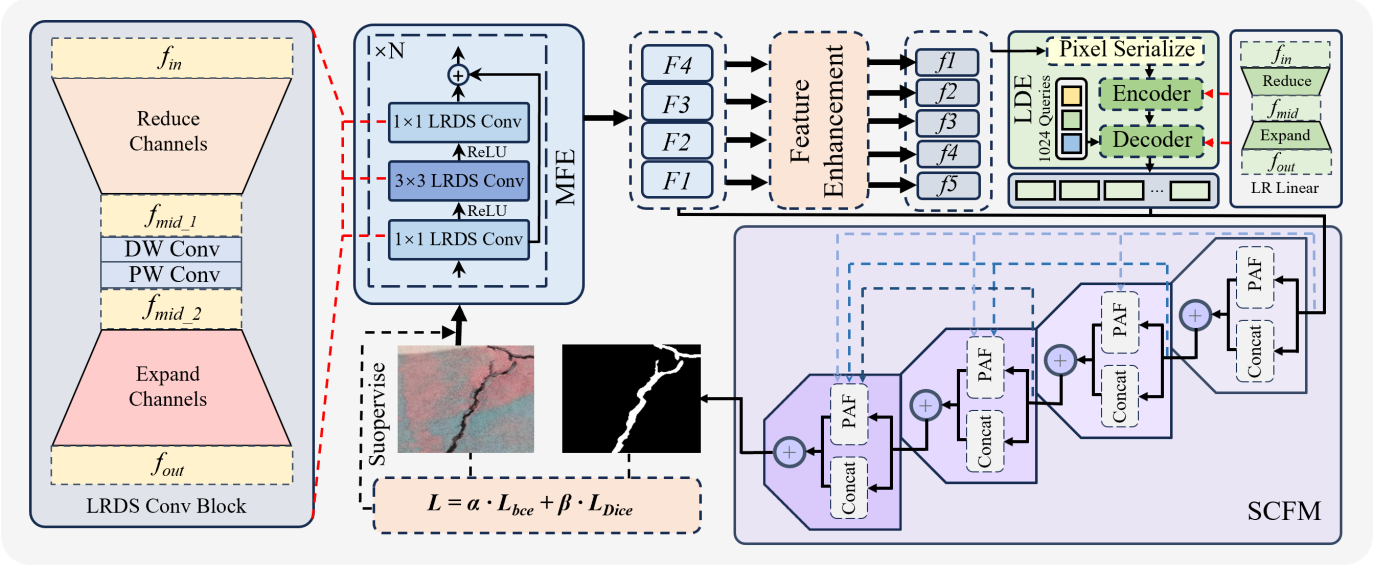


Fig. 2. General Architecture Diagram of CrackSCF Network. Crack images are first input into the MFE, generating four feature maps. After enhancement, five feature maps with unified channel numbers are obtained. The LDE module processes these maps to acquire pixel sequences rich in long-range correlations. The SCFM module then processes these sequences and the four layers of feature maps from the MFE. Through four stages, resulting in the segmentation output.

Thanks to the attention mechanism, transformers are particularly well-suited for handling targets with long-range dependencies and complex global structures, especially for cracks, which often have extensive spans and intricate shapes. Therefore, many researchers are amalgamating the outputs of CNNs and transformers for crack segmentation. Chen et al. [23] proposed TransUNet, a novel network architecture that effectively integrates long-range information and local features through a U-Net-like structure. Qi et al. [24] developed an end-to-end model based on Vision Transformer (ViT) and level set theory for segmenting defects in bridge pavement, achieving precise segmentation by amalgamating the outputs of two parallel decoders. Feng et al. [25] developed a shale crack segmentation network that combines CNN and Swin Transformer, utilizing Fast Fourier Transform (FFT) to merge feature maps from both, effectively suppressing high-frequency noise in the imaging process.

The aforementioned methods, while demonstrating the advantages of CNN-Transformer networks in processing pixel sequences and suppressing background noise, have limitations due to using only one method or branch for feature fusion. This reduces their ability to effectively perceive long-range dependencies and local patterns, causing some complex regions' local or long-range information to be overshadowed. Additionally, these methods excessively focus on performance, overlooking the substantial computational resources required for feature extraction and fusion, making them difficult to deploy on edge computing devices.

### B. Lightweight Networks

Deploying deep learning models on edge devices like smartphones and drones is trending. However, these devices have limited computing resources, making it challenging to use models with high parameter counts. Thus, compact model

design for lightweight modifications in size and speed is crucial. For example, Howard et al. [26] proposed MobileNet, an efficient model using depthwise separable convolutions to reduce computational load and parameter count, suitable for resource-constrained devices. Ma et al. [27] introduced ShuffleNet, providing practical design principles for efficient network architecture. Additionally, low-rank approximation compression, effective in fields like numerical linear algebra and image processing, is now used to compress deep learning network architectures. Zhang et al. [28] proposed a low-rank technique for neural networks that employs constrained optimization to determine the optimal low-rank approximation. Swaminathan et al. [29] introduced SLR, a sparse low-rank method that improves compression rates with sparse SVD matrices.

Recently, many researchers have combined model lightweighting techniques with crack segmentation models to enable real-time crack detection on edge devices. For example, Zhu et al. [30] designed RHACrackNet, a lightweight crack detection network integrating hybrid attention and residual blocks, enabling real-time detection on edge devices. Huang et al. [31] proposed a lightweight fusion attention module for road crack detection, ensuring high-precision crack extraction with rapid detection.

Although these lightweight models reduce computational resources, their emphasis on minimizing parameters results in limited model expressiveness, hindering their ability to effectively capture intricate patterns and features in the input data. This leads to unsatisfactory segmentation results. This imbalance between performance and lightweight design makes them unreliable in practical applications.

### III. METHODOLOGY

#### A. Network Architecture

As shown in Fig. 2, the CrackSCF network has three main components: a lightweight Multi-scale Feature Extractor (MFE), a Long-range Dependency Extractor (LDE), and a Staircase Cascaded Fusion Module (SCFM). The overall architecture of the network is shaped like a staircase, with feature maps of different scales progressively fused and upsampled. In this process, the advantages of CNNs and Transformers in feature extraction complement each other.

Specifically, for a given dataset, the crack images are first input into the MFE module, which is divided into four stages. In each stage, the extracted feature maps undergo a Feature Enhancement stage. Then, the LDE module processes these enhanced feature maps to obtain pixel sequences rich in long-range dependencies. Subsequently, the SCFM module receives these sequences along with the four layers of feature maps extracted by the MFE. After processing through four stages, the resolution is doubled at each stage while the number of channels is halved, ultimately resulting in the segmentation result.

Importantly, as shown in Fig. 3, using the original convolution operations results in high FLOPs and Params, especially in the SCFM module, reaching 73.36G and 9.71M, respectively. Replacing all convolutions with LRDS blocks significantly reduced FLOPs and Params, demonstrating the effectiveness of LRDS in model lightweighting.

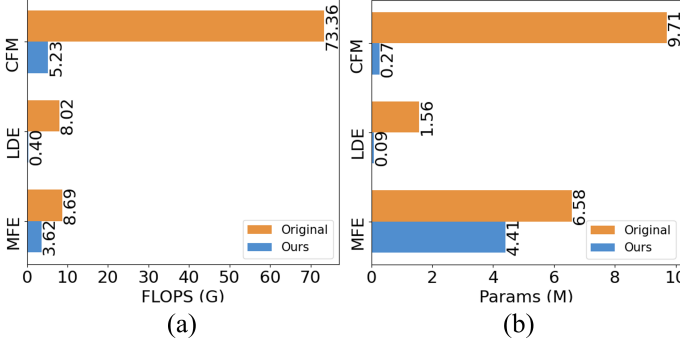


Fig. 3. Comparison of FLOPs and Params for each module using the original convolution and our proposed LRDS convolution block.

#### B. Lightweight Multi-scale Feature Extractor

As shown in Fig. 2 and Fig. 4, our designed LRDS block adopts a bottleneck-like structure. It comprises a Reduce layer, a depthwise convolution layer, a pointwise convolution layer, and an Expand layer. The input feature map first passes through the Reduce layer, reducing the input channels to  $C_m$ . It then goes through the depthwise convolution layer and the pointwise convolution layer, keeping the number of channels unchanged. Finally, the Expand layer increases the number of channels to  $C_d$ , producing the final output feature map.

Low-rank approximation decomposes a high-dimensional matrix into low-dimensional matrices, reducing computation complexity. In CNNs, it is applied to convolutional kernel responses, assuming these lie in a low-rank subspace.

Specifically, in the convolutional layer, we assume that its filter has a spatial size of  $k$  and a number of input channels of  $c$ . In computing the convolutional response, the filter is applied to a sub-tensor of the input tensor of shape  $k \times k \times c$ . Suppose this sub-tensor is  $t \in \mathbb{R}^{k^2 c + 1}$ , where we append a bias term at the end. The response at a position in the output,  $y \in \mathbb{R}^e$ , can be expressed as follows:

$$y = Wt \quad (1)$$

where  $e$  represents the number of filters and  $W$  is a  $e \times (k^2 c + 1)$  matrix. Assuming the vector  $y$  lies in a low-rank subspace, we can write it as  $y = U(y - y_1) + y_1$ , where  $U$  is a  $e \times e$  matrix of rank  $e_0$ , with  $e_0 < e$ .  $y_1$  is the mean vector of the response. Therefore, we can write the response as

$$y = UWt + b \quad (2)$$

where  $b = y_1 - Uy_1$  is the new bias. The rank of  $U$  is  $e_0$ , and it can be decomposed into two  $e \times e_0$  matrices  $J$  and  $K$  such that  $U = JK^T$ . We use  $W_1 = K^T W$  to denote a  $e_0 \times (k^2 c + 1)$  matrix, which corresponds to a set of  $e_0$  filters. Thus, we can rewrite the response as follows:

$$y = JW_1 t + b \quad (3)$$

The computational complexity of using Equation (3) is  $O(e_0 k^2 c) + O(ee_0)$ , whereas approximating  $y$  in the low-rank subspace using Equation (1) has a computational complexity of  $O(ek^2 c)$ . Given that  $O(ee_0) \ll O(e_0 k^2 c)$ , the complexity of using Equation (3) is  $\frac{e_0}{e}$  times that of using Equation (1).

Besides low-rank approximation, which reduces convolutional layer parameters and computational load, depthwise separable convolutions [26] also significantly reduce computational resources by decoupling spatial and channel dimensions. Therefore, we embedded depthwise and pointwise convolution layers in the LRDS block. Additionally, to better preserve local contextual information during feature extraction while avoiding excessive computational overhead, we incorporated strip pooling [32] technology into each bottleneck of ResNet50.

We constructed MFE by replacing all convolution operations in ResNet50 with LRDS convolution blocks.

#### C. Long-range Dependency Extractor

When extracting long-range dependencies of crack pixels, the deformable attention mechanism [33] adapts well to irregular structures. It calculates attention weights within a few sampled points, significantly reducing computational and memory overhead. Specifically, given an input  $x \in \mathbb{R}^{C \times H \times W}$ , let  $q$  denote a query element with query feature  $z_q$  and reference point coordinates  $(p_{qx}, p_{qy})$ , the deformable attention is calculated as:

$$\text{MSDeformAttn}(z_q, \hat{p}_q, \{x_c\}_{c=1}^C) = \sum_{h=1}^H W_h \left[ \sum_{c=1}^C \sum_{t=1}^T A_{hct} \cdot W'_h x_c (\phi_c(\hat{p}_q) + \Delta p_{hct}) \right] \quad (4)$$



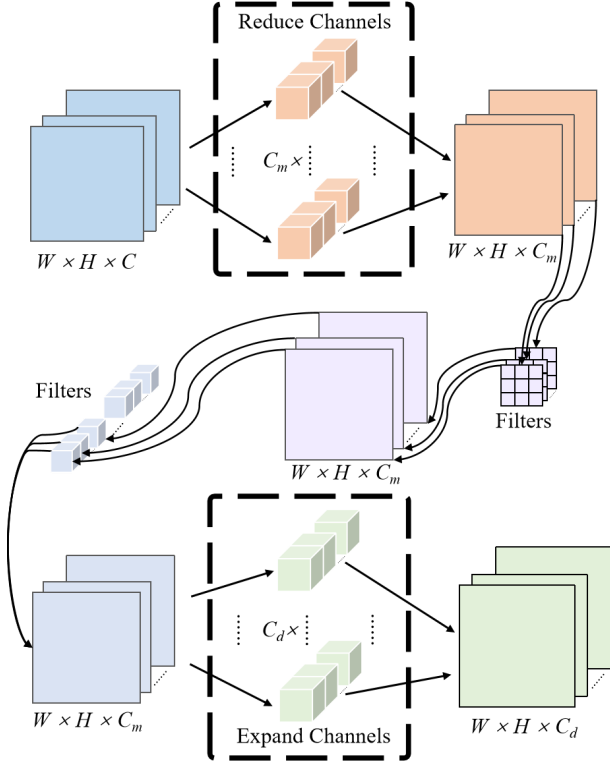


Fig. 4. Illustration of LRDS convolution block.

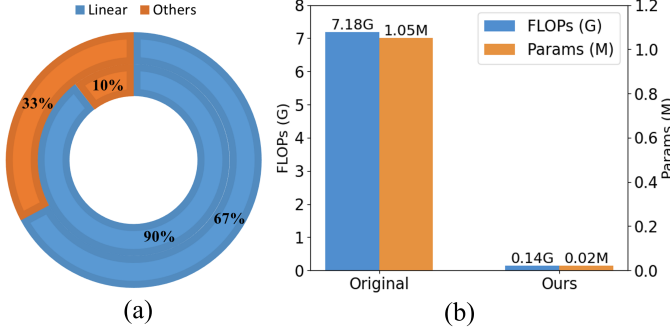


Fig. 5. Analysis of Computational Resources Required for Linear Operations. (a) shows the percentage of FLOPs and Params in the LDE module that use Original linear operations, with the inner circle showing the percentage that use FLOPs and the outer circle showing the percentage of Params. (b) Shows the comparison of FLOPs and Params for LDE before and after using LR Linear.

Where  $h$  represents the attention head,  $c$  represents the input feature layer, and  $t$  represents the sampling key point.  $\Delta p_{hcqt}$  and  $A_{hcqt}$  represent the offset and attention weight of the  $t$ -th sampling point in the  $c$ -th feature map and  $h$ -th attention head, respectively. The normalization is such that  $\sum_{c=1}^C \sum_{t=1}^T A_{hcqt} = 1$ . Here, normalized coordinates  $\hat{p} \in [0, 1]$  are used to represent the position of a reference point in the normalized feature map  $\phi_c(\hat{p}_q)$  rescales the normalized coordinates onto the  $c$ -th layer feature map.

The structure of LDE is shown in Fig. 2. Specifically, before the enhanced feature maps enters the LDE encoder, it is flattened into a long pixel sequence, aiding the deformable attention mechanism in extracting pixel dependencies. As

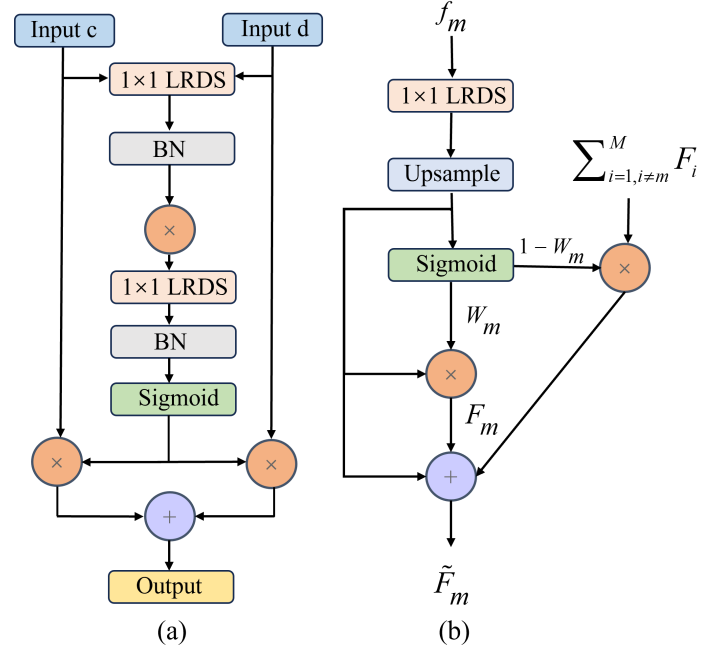


Fig. 6. Illustration of the PAF and SeFu.

shown in Fig. 5(a), Linear operations account for 90% of the FLOPs and 67% of the Params in the LDE module. To reduce these, we designed a lightweight Linear layer (LR Linear) using low-rank approximation, as shown in Fig. 2. We split the original Linear operation into two parts:  $f_m$  passes through the Reduce layer to get  $f_{mid}$  with 4 channels, then through the Expand layer to produce  $f_{out}$ . Replacing all Linear operations in the LDE with LR Linear reduced the parameters and computational load from 7.18G and 1.05M to 0.14G and 0.02M, as shown in Fig. 5(b).

#### D. Staircase Cascaded Fusion Module

The design of our SCFM structure is shown in Fig. 2. To enhance useful semantic features in the MFE and LDE branches and ensure effective semantic information is not buried, we improved the Pixel Attention Guided Fusion (PAF) module, inspired by PIDNet [34] and the need for model lightweighting. The structure of PAF is shown in Fig. 6(a). We denote the pixels in the feature maps of the two branches as  $\vec{v}_c$  and  $\vec{v}_d$ , respectively. Thus, the output can be expressed as:

$$\sigma = \text{Sigmoid}(f_c(\vec{v}_c) \cdot f_d(\vec{v}_d)) \quad (5)$$

where  $f_c$  and  $f_d$  denote pointwise convolution and batch normalization operations, respectively.  $\sigma$  indicates the probability that the two pixels belong to the same category. If  $\sigma$  is high, the model will trust  $\vec{v}_c$  more, indicating that its semantic features are more accurate, and vice versa. Thus, the output of PAF can be represented as:

$$\text{Output} = \sigma \vec{v}_c + (1 - \sigma) \vec{v}_d \quad (6)$$

To improve inference speed and reduce computational resource usage, all convolution operations in this module utilize

LRDS blocks. As seen in Fig. 3, using original convolution operations in the SCFM results in FLOPs and Params reaching 73.36G and 9.71M, respectively. Thus, lightweighting these operations is crucial. Replacing all convolution operations with LRDS blocks reduces FLOPs and Params by 92.87% and 97.22%, respectively, demonstrating the effectiveness of LRDS in network lightweighting. SCFM is divided into four stages, each with two fusion branches: the concat branch and the PAF branch. The concat operation retains complete information and diverse feature representations through direct concatenation, while the PAF module selectively fuses features through a pixel-guided attention mechanism, avoiding issues like buried feature information, information conflict, and redundancy. By perceiving the feature maps from the two branches, both local patterns of crack pixels and long-range dependencies can be comprehensively addressed.

To fully utilize the outputs of MFE and LDE and improve segmentation performance, SCFM incorporates the outputs from earlier stages and the associated MFE feature maps starting from the second stage. These are fused through the PAF module and processed by the Selective Feature Fusion (SeFu) module [7], which combines all PAF outputs before further operations. This approach effectively combines local semantic and long-range information, improving segmentation. The SeFu module structure is shown in Fig. 6(b).

#### E. Loss Function

The discrepancy between predictions and actual values is quantified by the loss function; a smaller value for this loss suggests superior model performance. Previously, Binary Cross-Entropy (BCE) [35] was often used, but it may not effectively distinguish the minority crack pixels in the image. Combining BCE with Dice loss [36] [37] addresses this issue. BCE improves the probability distribution for each pixel, while Dice loss maximizes the overlap between predictions and true labels, enhancing robustness against imbalanced data.

Our loss  $L$  can be calculated using Equation (7), which combines the above two loss functions for joint optimization.

$$L = \alpha \cdot L_{BCE} + \beta \cdot L_{Dice} \quad (7)$$

where  $\alpha$  and  $\beta$  are hyperparameters that determine the weights of the two losses. In our network,  $\alpha$  is set to 0.75 and  $\beta$  to 0.25.

### IV. EXPERIMENTS

In this section, we analyze the differences between our TUT dataset and other public datasets, describe the experimental setup, and compare methods and metrics. We then analyze results and model complexity, perform ablation experiments, and discuss current limitations and considerations.

#### A. Dataset Description

The previous works has used dataset scenarios that are relatively simple, such as cracks in cement or bitumen pavements only. These datasets have clear backgrounds and minimal interference, which cannot comprehensively evaluate the

performance of models. To tackle this problem, we created the TUT dataset to enable better segmentation across different scenarios. Detailed information and comparisons with other datasets are list in Table I.

The TUT dataset includes a substantial number of crack images captured with mobile phones, along with a smaller collection of images sourced from the internet. To ensure reliability in model training and testing, all images were manually annotated by several researchers to generate binary labels, and the best-annotated images were selected as the final labeled images. Unlike other datasets with clear backgrounds, the TUT dataset images have complex, noisy backgrounds and cracks of intricate shapes. This evaluates the model's capability to segment cracks in challenging conditions.

As list in Table I, our collected TUT dataset contains eight image scenarios, far more than the 1-2 scenarios of other public datasets, this allows for a more comprehensive evaluation of the model's performance in detecting cracks under various scenarios. Fig. ?? shows crack images in different scenarios and their binary labeled images. The crack pixel ratio in the TUT dataset is 3.16%, which is moderate. This ensures the model learns useful information without being hindered by too few crack pixels and prevents the model from overly relying on the crack pixel ratio when there are too many crack pixels.

As seen in Fig. ??, bitumen, cement, bricks, and plastic runways have extremely complex cracks due to their unique material properties. Particularly in plastic runways, both coarse and fine cracks are present, testing the model's generalization to different types of cracks. In images of tiles, metal materials, wind turbine blades, and underground pipelines, the crack shapes are relatively simple, but the backgrounds are very complex with various external interferences such as low light, irrelevant areas, and surface characteristics. This can easily result in false detections, thereby testing the model's ability to accurately extract crack areas from complex environments.

#### B. Implementation Details

1) *Experimental Settings*: The CrackSCF network is built on the PyTorch v2.1.1 deep learning framework and trained on an Ubuntu 20.04 server, featuring two Intel(R) Xeon(R) Platinum 8336C CPUs and eight Nvidia GeForce 4090 GPUs, each with 24GB VRAM. For training, the AdamW optimizer is utilized with an initial learning rate set at 0.0005, weight decay of 0.0001, batch size of one, and a total of 60 training epochs. The learning rate is reduced to one-tenth after 30 epochs as part of a decay strategy. The best-performing model parameters on the validation set are selected for testing. We compared the CrackSCF network with other SOTA methods on six datasets: CFD [38], GAPS509 [39], DeepCrack [19], Crack500 [20], CrackMap [40], and ours TUT dataset.

2) *Comparison Methods*: In evaluating model performance, we compared the CrackSCF network with 12 classic segmentation algorithms and the latest SOTA methods on different datasets. These methods include HED [44], UNet++ [45], Deeplabv3+ [46], AttuNet [47], RCF [48], RIND [49], UCT-Net [6], SFIAN [7], CT-crackseg [8], DTrCNet [9], Crackmer [10] and Simcrack [11].

TABLE I  
COMPARISON OF DIFFERENT CRACK DATASETS

No.	Datasets	Year	Num(train/val/test)	Resolution	Percentage of cracked pixels	Scenarios
1	CFD [38]	2016	118(76/11/31)	480 width and 320 height	1.60%	bitumen
2	GAPS509 [39]	2017	509(307/100/102)	540 width and 640 height	1.19%	bitumen
3	DeepCrack [19]	2019	537(300/100/247)	544 width and 384 height	3.54%	bitumen, cement
4	Crack500 [20]	2019	3368(1896/348/1124)	640 width and 360 height	6.01%	bitumen
5	CrackMap [40]	2023	120(72/12/36)	256 width and 256 height	4.10%	bitumen
6	AEL [20]	2019	58	768 width and 512 height	0.67%	bitumen
7	CrackTree206 [41]	2012	206	800 width and 600 height	0.32%	bitumen
8	LSCD [42]	2024	143	400 width and 400 height	3.18%	bitumen, cement
9	CrackSC [43]	2023	197	320 width and 480 height	2.02%	bitumen, cement
10	<b>TUT (Ours)</b>	2024	1408(987/139/282)	640 width and 640 height	3.16%	bitumen, cement, bricks, runways, metal, blades, pipelines, tiles

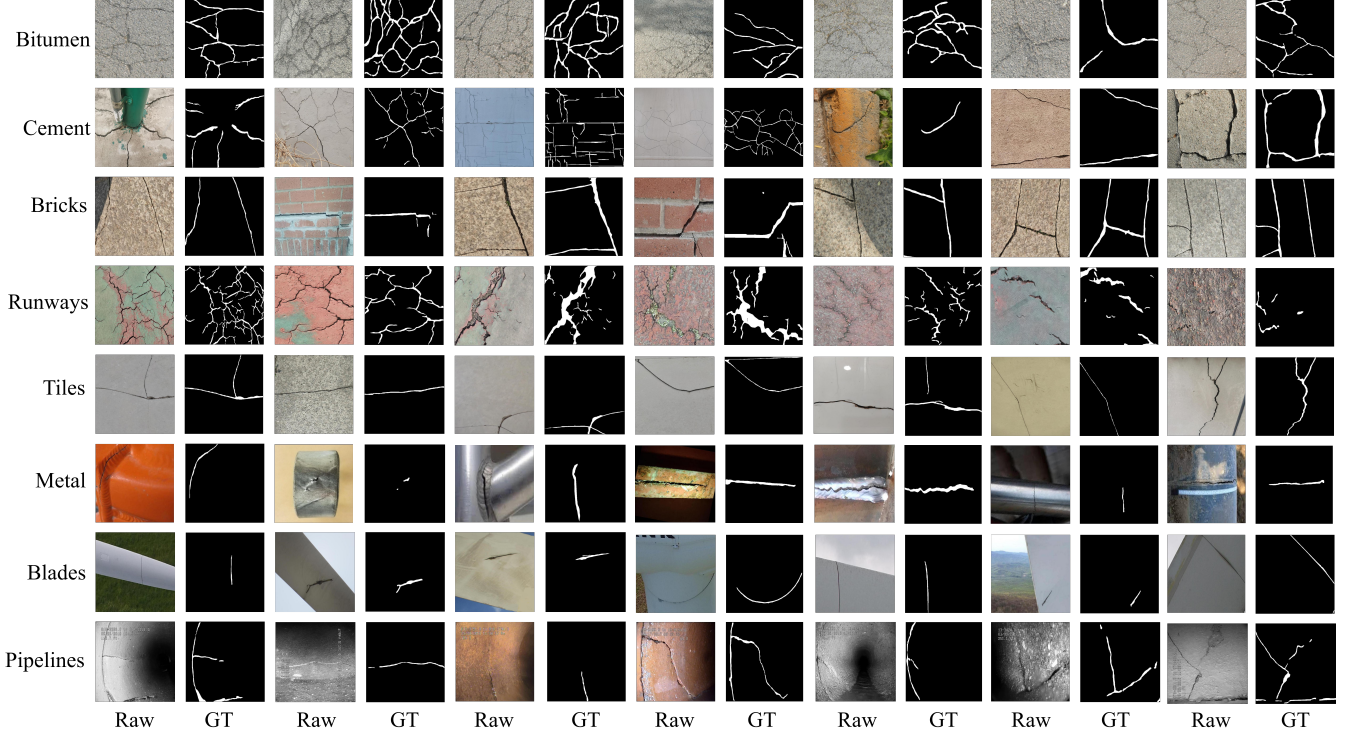


Fig. 7. Illustration of the images of each scenarios in the TUT dataset.

3) *Evaluation Metric*: To quantitatively evaluate the performance of our proposed crack segmentation model, we used six main metrics: Precision (P), Recall (R), F1 Score ( $F1 = \frac{2PR}{P+R}$ ), Mean Intersection over Union (mIoU), Optimal Dataset Scale (ODS), and Optimal Image Scale (OIS). Mean Intersection over Union (mIoU) measures the average ratio of the intersection and union of the predicted results and the true results. The calculation formula for mIoU is:

$$mIoU = \frac{1}{i+1} \sum_{a=0}^i \frac{p_{aa}}{\sum_{b=0}^i p_{ab} + \sum_{b=0}^i p_{ba} - p_{aa}} \quad (8)$$

where  $i$  is the number of classes,  $a$  denotes the true value,  $b$  denotes the predicted value, and  $p_{ab}$  represents the number of pixels predicted as  $a$  for  $b$ . Given that our crack segmentation task involves binary classification, we set  $i = 1$ .

Optimal Dataset Scale (ODS) indicates the optimal segmentation performance metric obtained when a fixed threshold  $t$

is selected over the entire dataset. It is defined as:

$$ODS = \max_t \frac{2 \cdot P_t \cdot R_t}{P_t + R_t} \quad (9)$$

Optimal Image Scale (OIS) indicates the optimal segmentation performance metric obtained when an optimal threshold  $t$  is selected for each image individually. It is defined as:

$$OIS = \frac{1}{N} \sum_{a=1}^N \max_t \frac{2 \cdot P_{t,a} \cdot R_{t,a}}{P_{t,a} + R_{t,a}} \quad (10)$$

where  $N$  represents the total number of images.

### C. Comparison with the SOTA methods

Our proposed method, CrackSCF, was compared with 12 other methods across five public datasets and our own TUT dataset. Table II displays the comparison results for the five

TABLE II

COMPARISON OF RESULTS BETWEEN CRACKSCF AND OTHER METHODS ON THE PUBLIC DATASET AND THE TUT DATASET. RESULTS ARE HIGHLIGHTED WITH THE BEST IN RED AND THE SECOND-BEST IN BLUE

Methods	CFD						GAPS509						Crack500					
	ODS	OIS	P	R	F1	mIoU	ODS	OIS	P	R	F1	mIoU	ODS	OIS	P	R	F1	mIoU
HED	0.6276	0.6494	0.5467	0.7374	0.6279	0.7240	0.4014	0.4509	0.4300	0.4624	0.4456	0.6282	0.6191	0.6537	0.6150	0.7281	0.6668	0.7140
UNet++	0.6586	0.6836	0.5995	0.7608	0.6706	0.7432	0.6255	0.6484	0.6160	0.6684	0.6411	0.7300	0.6965	0.7274	0.6989	0.7805	0.7374	0.7605
DeeplabV3+	0.6910	0.7084	0.6264	<b>0.7730</b>	0.6920	0.7709	0.6160	0.6425	0.6050	0.6669	0.6345	<b>0.7378</b>	0.6943	0.7211	0.6970	0.7569	0.7257	0.7746
AttuNet	0.6710	0.6870	0.6240	0.7220	0.6694	0.7576	0.5955	0.6174	0.5924	0.6519	0.6208	0.7247	0.6586	0.6890	0.6490	0.7608	0.7005	0.7543
RCF	0.6434	0.6624	0.5792	0.7348	0.6478	0.7343	0.4532	0.4817	0.4420	0.5428	0.4872	0.6472	0.6054	0.6361	0.6037	0.7136	0.6540	0.7068
RIND	0.6858	0.7021	0.6456	0.7534	0.6954	0.7592	0.5505	0.6023	0.4959	0.6494	0.5623	0.6909	0.6469	0.6483	0.6998	0.7245	0.7119	0.7381
UCTNet	0.6587	0.7006	0.6701	0.7205	0.6944	0.7479	0.5835	0.6188	0.5709	0.6752	0.6187	0.7107	<b>0.7147</b>	0.7265	0.6887	0.7843	0.7302	0.7674
SFIAN	0.7040	0.7159	0.6657	0.7512	0.7058	0.7684	0.6087	0.6320	0.6061	0.6451	0.6250	0.7198	0.6977	<b>0.7348</b>	0.6983	0.7742	0.7343	0.7604
CT-crackseg	0.7122	0.7179	<b>0.6896</b>	0.7438	0.7157	0.7738	0.6029	0.6075	0.5693	0.6804	0.6199	0.7165	0.6941	0.7059	0.6940	0.7748	0.7322	0.7591
DTrCNet	0.7079	0.7123	0.6774	0.7486	0.7112	0.7710	0.6211	0.6276	<b>0.6277</b>	0.6592	0.6431	0.7272	0.7012	0.7241	0.6527	<b>0.8280</b>	0.7357	0.7627
Crackmer	0.6751	0.6752	0.6370	0.7237	0.6776	0.7503	0.4593	0.4642	0.6144	0.4663	0.5302	0.6581	0.6933	0.7097	0.6985	0.7572	0.7267	0.7591
SimCrack	<b>0.7152</b>	<b>0.7204</b>	0.6883	0.7557	<b>0.7204</b>	<b>0.7756</b>	<b>0.6408</b>	<b>0.6471</b>	0.6171	<b>0.6997</b>	<b>0.6558</b>	0.7368	0.7127	0.7308	<b>0.7093</b>	0.7984	<b>0.7516</b>	<b>0.7715</b>
Ours	<b>0.7335</b>	<b>0.7376</b>	<b>0.6967</b>	<b>0.7848</b>	<b>0.7383</b>	<b>0.7864</b>	<b>0.6492</b>	<b>0.6552</b>	<b>0.6459</b>	<b>0.6812</b>	<b>0.6631</b>	<b>0.7411</b>	<b>0.7226</b>	<b>0.7353</b>	<b>0.7213</b>	<b>0.7922</b>	<b>0.7551</b>	<b>0.7764</b>
Methods	CrackMap						DeepCrack						TUT (Ours)					
	ODS	OIS	P	R	F1	mIoU	ODS	OIS	P	R	F1	mIoU	ODS	OIS	P	R	F1	mIoU
HED	0.6022	0.6240	0.5281	0.7063	0.6043	0.7026	0.7552	0.8237	0.7231	0.7678	0.7448	0.8007	0.6960	0.7254	0.7080	0.7431	0.7251	0.7683
UNet++	0.7030	0.7222	0.6773	0.7209	0.6984	0.7631	0.8419	0.8893	0.8474	0.8533	0.8503	0.8621	0.7702	0.7948	0.7725	0.7974	0.7848	0.8160
DeeplabV3+	0.6617	0.6793	0.5853	0.7532	0.6587	0.7460	0.7727	0.8354	0.7363	0.8323	0.7813	0.8565	0.7504	0.7777	0.7155	0.8231	0.7655	0.8177
AttuNet	0.6618	0.6773	0.6233	0.6970	0.6581	0.7454	0.8153	0.8379	0.8066	0.8069	0.8068	0.8578	0.7539	0.7795	0.7558	0.7945	0.7747	0.8204
RCF	0.5552	0.5683	0.4590	0.7164	0.5595	0.6758	0.7666	0.8376	0.7423	0.7611	0.7516	0.8110	0.6821	0.7138	0.7106	0.6877	0.6990	0.7598
RIND	0.6745	0.6943	0.6023	0.7586	0.6699	0.7425	0.8087	0.8267	0.7896	<b>0.8920</b>	0.8377	0.8391	0.7531	0.7891	0.7872	0.7665	0.7767	0.8051
UCTNet	0.6104	0.6195	0.5653	0.6748	0.6152	0.7079	0.8357	0.8579	0.8217	0.8857	0.8525	0.8564	0.7569	0.7670	0.8201	0.7667	0.7925	0.8110
SFIAN	0.7200	0.7465	0.6715	0.7668	0.7160	0.7748	0.8616	<b>0.8928</b>	0.8549	0.8692	0.8620	0.8776	0.7290	0.7513	0.7715	0.7367	0.7537	0.7896
CT-crackseg	0.7289	0.7373	0.6911	0.7669	0.7270	0.7785	<b>0.8819</b>	0.8904	<b>0.9011</b>	0.8895	<b>0.8952</b>	<b>0.8925</b>	0.7940	0.7996	<b>0.8202</b>	0.8195	0.8199	0.8301
DTrCNet	0.7328	0.7413	0.6912	<b>0.7681</b>	0.7276	0.7812	0.8473	0.8512	0.8905	0.8251	0.8566	0.8661	0.7987	0.8073	0.7972	<b>0.8441</b>	0.8202	0.8331
Crackmer	0.7395	0.7437	0.7229	0.7467	0.7346	0.7860	0.8712	0.8785	0.8946	0.8783	0.8864	0.8844	0.7429	0.7640	0.7501	0.7656	0.7578	0.7966
SimCrack	<b>0.7559</b>	<b>0.7625</b>	<b>0.7380</b>	0.7672	<b>0.7523</b>	<b>0.7963</b>	0.8570	0.8722	0.8984	0.8549	0.8761	0.8744	<b>0.7984</b>	<b>0.8090</b>	0.8051	0.8371	<b>0.8208</b>	<b>0.8334</b>
Ours	<b>0.7595</b>	<b>0.7651</b>	<b>0.7390</b>	<b>0.7708</b>	<b>0.7546</b>	<b>0.7987</b>	<b>0.8914</b>	<b>0.8963</b>	<b>0.9147</b>	<b>0.9013</b>	<b>0.9079</b>	<b>0.9001</b>	<b>0.8202</b>	<b>0.8266</b>	<b>0.8282</b>	<b>0.8484</b>	<b>0.8382</b>	<b>0.8473</b>

public datasets, while Fig. 8 illustrates the visual results of all methods on these datasets.

1) *Results on the CFD dataset:* The crack areas in the CFD dataset are very slender, testing the model's sensitivity to fine-grained crack pixels. As list in Table II, our proposed CrackSCF attained the best results across all metrics for the CFD dataset. Specifically, on ODS, OIS, P, R, F1, and mIoU, it outperformed the second-best methods by 0.48%, 0.34%, 0.14%, 0.35%, 0.31%, and 0.30%, respectively. Notably, SimCrack [11] achieved the second-best performance on all metrics except for P and R, only behind our method. However, as seen in Fig. 8, its actual segmentation performance is not satisfactory, while our method achieves high-quality segmentation results on various fine-grained crack pixels. Other methods, such as UCTNet and DTrCNet [9], tend to misdetect background noise or miss key detail areas of crack pixels.

2) *Results on the GAPS509 dataset:* Unlike the CFD dataset, the GAPS509 dataset contains not only finer cracks but also some irrelevant background interference, testing the model's ability to extract crack areas under high interference conditions. As list in Table II, our method achieved the highest performance on all metrics except R. Although SimCrack [11] achieved 0.6997 on the R metric, leading our method by about 2.72%, its P metric was 0.6171, far lower than our method. The highest F1 score obtained by our method indicates a good balance between P and R. Specifically, our method outperformed the second-best methods on ODS, OIS, P, F1, and mIoU by 1.31%, 1.25%, 2.90%, 1.11%, and 0.45%,

respectively. Additionally, as seen in Fig. 8, our method almost perfectly avoids irrelevant background noise, while most other methods falsely detect irrelevant backgrounds and perform worse in segmenting crack pixel areas compared to our method.

3) *Results on the DeepCrack dataset:* The cracks in the DeepCrack dataset are often relatively wide, testing the model's ability to extract a large range of crack pixels. As list in Table II, our method achieved the highest results on all metrics for the DeepCrack dataset. Specifically, our method outperformed the second-best methods on ODS, OIS, P, R, F1, and mIoU by 1.08%, 0.39%, 1.51%, 1.04%, 1.42%, and 0.85%, respectively. Notably, CT-crackseg also achieved good results on this dataset, but as seen in Fig. 8, its segmentation performance on detailed cracks is not as good as our method, indicating that our method can effectively handle crack details.

4) *Results on the Crack500 dataset:* Similar to the DeepCrack dataset, the Crack500 dataset also has relatively wide crack areas, but its structure is more complex, posing higher requirements on model performance. As list in Table II, our method achieved the best results on five metrics for the Crack500 dataset, except for R. It outperformed the second-best methods on ODS, OIS, P, F1, and mIoU by 1.11%, 0.07%, 1.69%, 0.47%, and 0.64%, respectively. Although DTrCNet [9] leads on the R metric, our method surpasses it on the P metric by 10.51%. The highest F1 score achieved by our method indicates a good balance between P and R. Additionally, as seen in Fig. 8, our method does not produce false detections in irrelevant background areas, whereas other methods either



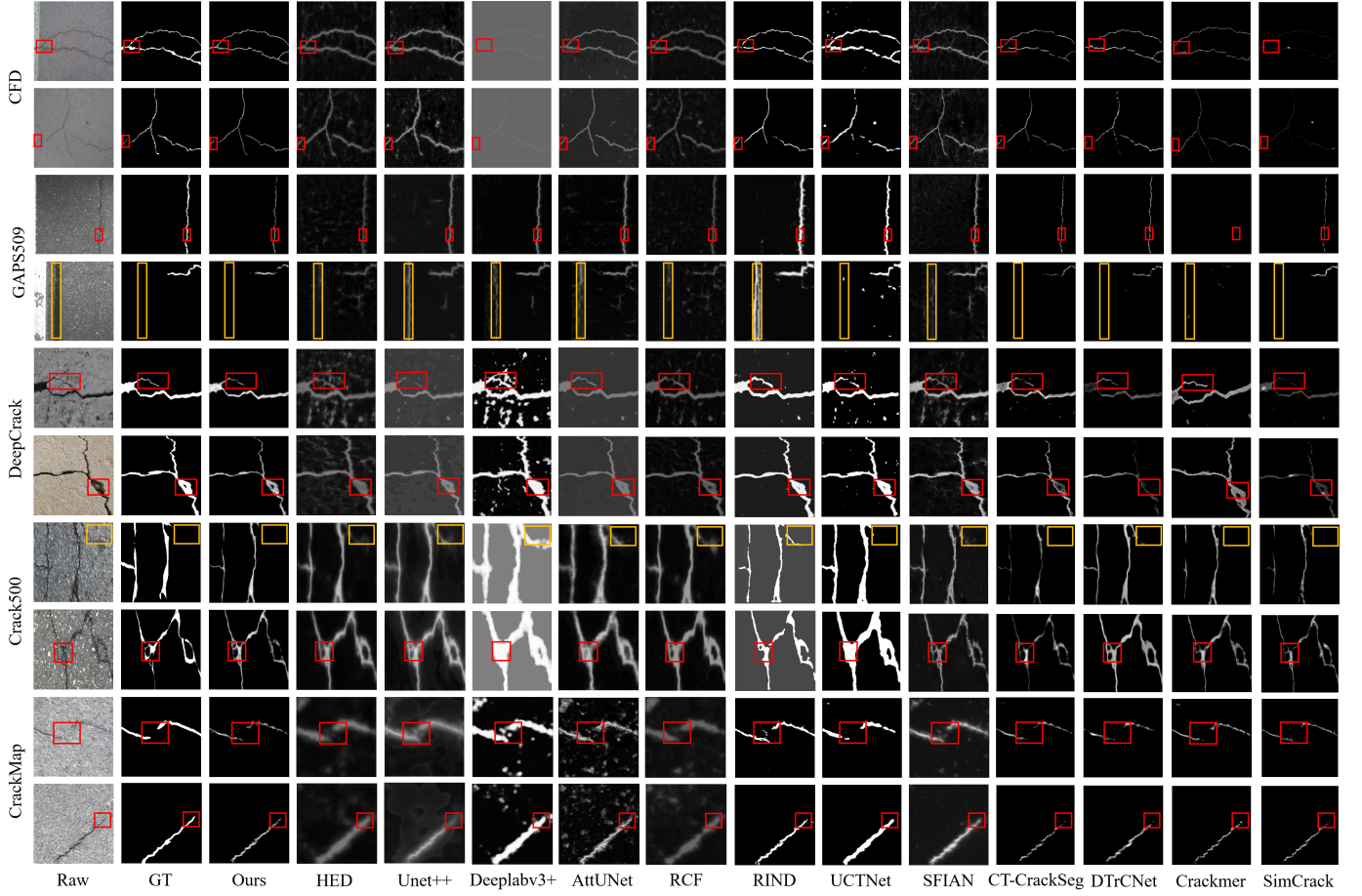


Fig. 8. Visualization results of CrackSCF and other methods on public datasets. Key areas are highlighted with red boxes to indicate easily missed crack pixels and yellow boxes to indicate easily misdetected non-crack areas.

produce false detections or lack detailed segmentation in crack areas.

5) *Results on the CrackMap dataset:* Similar to the CFD dataset, the cracks in the CrackMap dataset are also relatively slender. As list in Table II, our method leads all other methods on all metrics, outperforming the second-best methods on ODS, OIS, P, R, F1, and mIoU by 0.48%, 0.34%, 0.14%, 0.35%, 0.31%, and 0.30%, respectively. Notably, SimCrack [11] achieved the second-best results on this dataset, but as seen in Fig. 8, SimCrack’s segmentation performance on the crack tips is not satisfactory, whereas our method effectively identifies these pixels.

6) *Results on the TUT dataset:* Fig. 9 shows the visual results of all methods on the TUT dataset. We manually highlighted easily missed crack pixel areas with red boxes and misdetected non-crack pixel areas with yellow boxes. As list in Table II, our method achieved excellent results on the TUT dataset, leading in all metrics. Specifically, it outperformed the second-best methods on ODS, OIS, P, R, F1, and mIoU by 2.73%, 2.18%, 0.98%, 0.51%, 2.12%, and 1.67%, respectively. SimCrack [11] achieved the second-best results on ODS, OIS, F1, and mIoU, but as seen in Fig. 9, its segmentation performance on some key details has room for improvement compared to our method.

Furthermore, most methods fail to suppress irrelevant back-

ground noise. In images of metal materials and turbine blades, our method effectively removes noise and accurately segments crack regions. In pipeline scenarios, our method can filter out timestamp watermarks, thanks to SCFM, which enables the model to focus on irregular, slender crack structures rather than irrelevant watermarks. Our method demonstrates excellent robustness and versatility, resulting in high-quality crack segmentation maps and adapting well to different scenarios.

#### D. Complexity Analysis

To assess our LRDS block’s efficacy, we analyzed its computational and parameter efficiency using three metrics: floating point operations (FLOPs), number of parameters (Params), and frames per second (FPS). FLOPs quantify computational load, reflecting demand during inference. Params measure storage requirements, reflecting trainable and stored parameters. FPS gauges real-time processing, indicating frames processed per second under specific hardware conditions.

Table III presents our method’s performance alongside other comparisons in terms of FLOPs, Params, and FPS. Our approach achieves notably low values in FLOPs (9.26G) and Params (4.79M), surpassing the second-best by 38.01% and 18.81%, respectively. This underscores our algorithm’s efficiency, making it suitable for implementation on resource-constrained edge devices. In FPS, our model achieves the



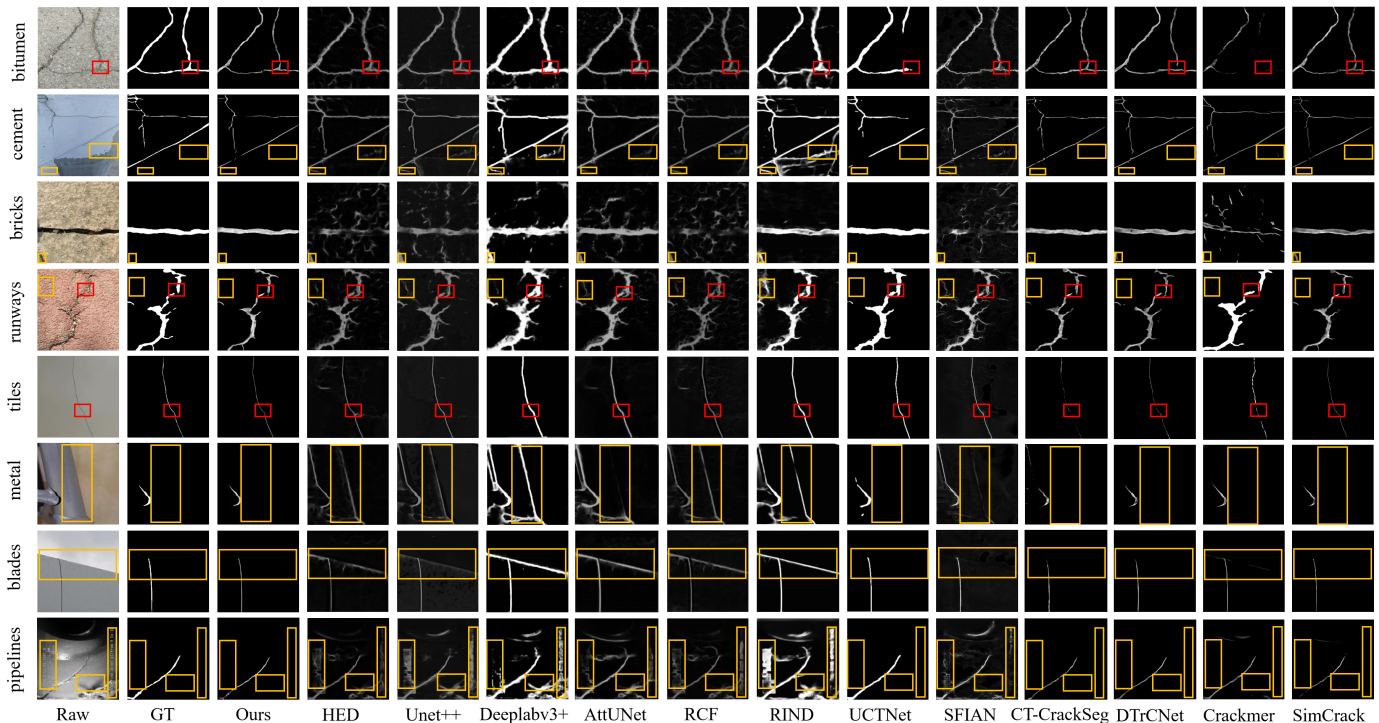


Fig. 9. Visualization results of CrackSCF and other methods on TUT dataset. Key areas are highlighted with red boxes to indicate easily missed crack pixels and yellow boxes to indicate easily misdetected non-crack areas.

second-best performance, processing 36 frames per second, trailing only behind the speed-focused DTrCNet [9]. This highlights our model’s robust real-time capability, crucial for prompt crack image segmentation in practical applications. Overall, our model combines minimal parameters and computational load with competitive processing speed, ensuring effective deployment on devices like smartphones, drones, and other portable platforms.

TABLE III  
COMPARISON OF THE COMPLEXITY OF CRACKSCF WITH OTHER METHODS. RESULTS ARE HIGHLIGHTED WITH THE BEST IN RED AND THE SECOND-BEST IN BLUE

Methods	FLOPs ↓	Params ↓	FPS ↑
HED	80.35G	14.72M	33
RCF	115.54G	15.52M	30
RIND	695.77G	59.39M	11
UCTNet	171.77G	66.22M	12
UNet++	139.61G	9.16M	22
DeeplabV3+	88.53G	59.34M	29
AttuNet	541.34G	57.16M	24
SFIAN	52.36G	13.63M	35
CT-crackseg	39.47G	22.88M	28
DTrCNet	123.20G	63.45M	47
SimCrack	70.66G	29.58M	29
Crackmer	14.94G	5.90M	31
Ours	9.26G	4.79M	36

### E. Ablation Analysis

To evaluate the advantages of our LRDS block compared to other convolution operations, we performed ablation experiments on the TUT dataset, as list in Table IV. On six metrics, our method slightly outperforms those using only

depthwise separable or low-rank approximation convolutions. Our method reduces FLOPs by 61.26% and 56.69%, respectively, and Params by 0.16M compared to the low-rank approximation block, achieving the highest FPS. Compared to original convolution operations, our method reduces FLOPs and Params by 89.70% and 73.19%, respectively, without degrading performance. These results indicate that our convolution block effectively reduces computational load and utilizes parameters while maintaining or improving segmentation performance, enhancing processing speed and benefiting lightweight model design.

To demonstrate the effectiveness of SCFM in fusing local detail features and long-range information, we performed ablation experiments on the TUT dataset, as list in Table V. Our method, using Concat and PAF dual-branch feature fusion, achieves the best results across all six segmentation metrics. Using only the PAF branch results in a 1.06% drop in the F1 score. While SCFM slightly increases parameter count, computational load, and inference speed, it significantly improves segmentation performance. These results indicate that our module effectively balances performance and efficiency.

Table VI shows the results of ablation experiments on different weight proportions of the two sub-losses in the loss function. As shown, a Dice loss to BCE loss ratio of 1:3 yields the highest values in five metrics: ODS, OIS, R, F1, and mIoU. Although the P metric is 0.80% lower than using only BCE loss, the F1 metric improves by 2.58%, indicating a better balance between P and R. Therefore, we use this ratio during training. In summary, a Dice loss to BCE loss ratio of 1:3 not only enhances pixel-level performance but also improves the global segmentation of crack areas, achieving

TABLE IV  
COMPARISON OF CRACKSCF USING LRDS BLOCKS WITH NETWORKS USING OTHER CONVOLUTIONS. RESULTS ARE HIGHLIGHTED WITH THE BEST IN RED AND THE SECOND-BEST IN BLUE

Method	ODS	OIS	P	R	F1	mIoU	FLOPs ↓	Params ↓	FPS ↑
CrackSCF_Original	0.8145	0.8193	<b>0.8294</b>	0.8398	<b>0.8346</b>	0.8437	90.06G	17.86M	23
CrackSCF_DS	0.8117	0.8166	0.8239	0.8364	0.8301	0.8417	23.91G	8.38M	<b>35</b>
CrackSCF_LR	<b>0.8154</b>	<b>0.8220</b>	0.8220	<b>0.8451</b>	0.8334	<b>0.8441</b>	21.38G	4.63M	30
CrackSCF_LRDS	<b>0.8202</b>	<b>0.8266</b>	<b>0.8282</b>	<b>0.8484</b>	<b>0.8382</b>	<b>0.8473</b>	<b>9.26G</b>	<b>4.79M</b>	<b>36</b>

TABLE V  
COMPARISON OF CRACKSCF NETWORKS USING SCFM, CONCAT AND PAF. RESULTS ARE HIGHLIGHTED WITH THE BEST IN RED AND THE SECOND-BEST IN BLUE

Method	ODS	OIS	P	R	F1	mIoU	FLOPs ↓	Params ↓	FPS ↑
CrackSCF_Concat	0.8019	0.8092	0.8228	0.8209	0.8219	0.8359	<b>7.21G</b>	<b>4.71M</b>	<b>42</b>
CrackSCF_PAF	<b>0.8137</b>	<b>0.8202</b>	<b>0.8282</b>	<b>0.8297</b>	<b>0.8293</b>	<b>0.8427</b>	<b>8.24G</b>	<b>4.72M</b>	<b>39</b>
CrackSCF_SCFM	<b>0.8202</b>	<b>0.8266</b>	<b>0.8289</b>	<b>0.8484</b>	<b>0.8382</b>	<b>0.8473</b>	9.26G	4.79M	36

TABLE VI  
COMPARISON OF RESULTS OF CRACKSCF NETWORKS TRAINED WITH DIFFERENT LOSS RATIOS

Dice : BCE	ODS	OIS	P	R	F1	mIoU
1 : 5	0.8129	0.8203	0.8217	<b>0.8458</b>	<b>0.8336</b>	0.8424
1 : 4	0.8049	0.8145	0.8116	0.8365	0.8239	0.8368
1 : 3	<b>0.8202</b>	<b>0.8266</b>	0.8282	<b>0.8484</b>	<b>0.8382</b>	<b>0.8473</b>
1 : 2	<b>0.8146</b>	<b>0.8211</b>	0.8227	0.8435	0.8330	<b>0.8438</b>
1 : 1	0.8136	0.8204	0.8231	0.8436	0.8332	0.8431
Only BCE	0.8003	0.8056	<b>0.8349</b>	0.8004	0.8173	0.8332
Only Dice	0.8107	0.8165	<b>0.8302</b>	0.8265	0.8283	0.8409

achieve faster inference speeds while maintaining a good balance between segmentation performance and model lightweighting.

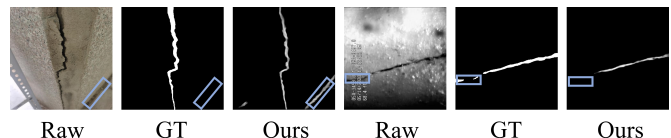


Fig. 10. Examples of CrackSCF misdetections and misses. The critical regions are marked with blue boxes.

superior segmentation performance.

#### F. Limitations and Discussions

Through these experiments, we found that SCFM effectively perceives and fuses local details and long-range pixel dependencies. Our network excels in various metrics on public datasets with simple scenes and performs exceptionally on the complex TUT dataset. The lightweight LRDS block minimizes parameters and computational load, facilitating deployment on resource-constrained devices like drones and smartphones. However, our network has several limitations, as follows:

- 1) Although our method generally achieves good crack segmentation with effective background noise suppression, as shown in the Fig. 10, our model occasionally misdetects noise regions that resemble cracks in some images. It also fails to detect watermark occlusions with colors similar to the background. Therefore, it is essential to enhance modules such as MFE and LDE to improve the model's capability to perceive and extract features from critical noise and occlusion areas, thereby further increasing its robustness and stability in complex scenarios.
- 2) Despite our method achieves the minimum parameter count and computational load, there is still room for improvement in inference speed. For example, our network achieves a processing speed of 36 frames per second, but the DTrCNet [9], which focuses more on inference speed, attains a faster speed of 47 frames per second. Therefore, it is necessary to further simplify convolution operations or the network's complexity to

#### V. CONCLUSION

This paper proposes a staircase cascaded fusion network (CrackSCF) for pixel-level crack detection. We developed SCFM to fuse the local patterns processed by MFE and the pixel dependencies processed by LDE. Additionally, we introduced the lightweight convolution block LRDS to replace all convolution operations in the network, effectively reducing the substantial parameter count and computational load required for training and inference. Furthermore, to comprehensively evaluate our model's robustness and stability across various complex scenarios, we collected the TUT dataset, which includes eight types of crack scenes. Experimental results show that our method performs best on five public datasets and the TUT dataset, particularly excelling in background noise suppression and fine crack segmentation. The computational load and parameter count are reduced to 9.26G and 4.79M, respectively, with an inference speed of up to 36 frames per second.

In future work, we plan to continue designing an improved SCFM to better fuse and enhance local information and global context for superior segmentation results. Additionally, we will further pursue network lightweighting to reduce computational resource requirements and achieve higher inference speeds, aiming to deploy our model on mobile devices for better real-world applications.

#### REFERENCES

- [1] R. Ali, J. H. Chuah, M. S. A. Talip, N. Mokhtar, and M. A. Shoaib, "Structural crack detection using deep con-

- volutional neural networks,” *Automation in Construction*, vol. 133, p. 103989, 2022.
- [2] H. Zhang, A. A. Zhang, Z. Dong, A. He, Y. Liu, Y. Zhan, and K. C. Wang, “Robust semantic segmentation for automatic crack detection within pavement images using multi-mixing of global context and local image features,” *IEEE Transactions on Intelligent Transportation Systems*, 2024.
  - [3] J. Zhou, P. S. Huang, and F.-P. Chiang, “Wavelet-based pavement distress detection and evaluation,” *Optical Engineering*, vol. 45, no. 2, pp. 027 007–027 007, 2006.
  - [4] T. Yamaguchi, S. Nakamura, R. Saegusa, and S. Hashimoto, “Image-based crack detection for real concrete surfaces,” *IEEJ Transactions on Electrical and Electronic Engineering*, vol. 3, no. 1, pp. 128–135, 2008.
  - [5] H. Oliveira and P. L. Correia, “Automatic road crack segmentation using entropy and image dynamic thresholding,” in *2009 17th European Signal Processing Conference*. IEEE, 2009, pp. 622–626.
  - [6] H. Wang, P. Cao, J. Wang, and O. R. Zaiane, “Uctransnet: rethinking the skip connections in u-net from a channel-wise perspective with transformer,” in *Proceedings of the AAAI conference on artificial intelligence*, vol. 36, no. 3, 2022, pp. 2441–2449.
  - [7] X. Cheng, T. He, F. Shi, M. Zhao, X. Liu, and S. Chen, “Selective feature fusion and irregular-aware network for pavement crack detection,” *IEEE Transactions on Intelligent Transportation Systems*, 2023.
  - [8] H. Tao, B. Liu, J. Cui, and H. Zhang, “A convolutional-transformer network for crack segmentation with boundary awareness,” in *2023 IEEE International Conference on Image Processing (ICIP)*. IEEE, 2023, pp. 86–90.
  - [9] C. Xiang, J. Guo, R. Cao, and L. Deng, “A crack-segmentation algorithm fusing transformers and convolutional neural networks for complex detection scenarios,” *Automation in Construction*, vol. 152, p. 104894, 2023.
  - [10] J. Wang, Z. Zeng, P. K. Sharma, O. Alfarraj, A. Tolba, J. Zhang, and L. Wang, “Dual-path network combining cnn and transformer for pavement crack segmentation,” *Automation in Construction*, vol. 158, p. 105217, 2024.
  - [11] A. Jaziri, M. Mundt, A. Fernandez, and V. Ramesh, “Designing a hybrid neural system to learn real-world crack segmentation from fractal-based simulation,” in *Proceedings of the IEEE/CVF Winter Conference on Applications of Computer Vision*, 2024, pp. 8636–8646.
  - [12] Z. Qu, W. Chen, S.-Y. Wang, T.-M. Yi, and L. Liu, “A crack detection algorithm for concrete pavement based on attention mechanism and multi-features fusion,” *IEEE Transactions on Intelligent Transportation Systems*, vol. 23, no. 8, pp. 11 710–11 719, 2021.
  - [13] H. Chu, W. Chen, and L. Deng, “Cascade operation-enhanced high-resolution representation learning for meticulous segmentation of bridge cracks,” *Advanced Engineering Informatics*, vol. 61, p. 102508, 2024.
  - [14] A. Dosovitskiy, L. Beyer, A. Kolesnikov, D. Weissenborn, X. Zhai, T. Unterthiner, M. Dehghani, M. Minderer, G. Heigold, S. Gelly *et al.*, “An image is worth 16x16 words,” *arXiv preprint arXiv:2010.11929*, vol. 7, 2020.
  - [15] Z. Liu, Y. Lin, Y. Cao, H. Hu, Y. Wei, Z. Zhang, S. Lin, and B. Guo, “Swin transformer: Hierarchical vision transformer using shifted windows,” in *Proceedings of the IEEE/CVF international conference on computer vision*, 2021, pp. 10 012–10 022.
  - [16] A. Vaswani, N. Shazeer, N. Parmar, J. Uszkoreit, L. Jones, A. N. Gomez, Ł. Kaiser, and I. Polosukhin, “Attention is all you need,” *Advances in neural information processing systems*, vol. 30, 2017.
  - [17] H. Chu, L. Deng, H. Yuan, L. Long, and J. Guo, “A transformer and self-cascade operation-based architecture for segmenting high-resolution bridge cracks,” *Automation in Construction*, vol. 158, p. 105194, 2024.
  - [18] J. Dong, N. Wang, H. Fang, W. Guo, B. Li, and K. Zhai, “Mfafnet: An innovative crack intelligent segmentation method based on multi-layer feature association fusion network,” *Advanced Engineering Informatics*, vol. 62, p. 102584, 2024.
  - [19] Y. Liu, J. Yao, X. Lu, R. Xie, and L. Li, “Deepcrack: A deep hierarchical feature learning architecture for crack segmentation,” *Neurocomputing*, vol. 338, pp. 139–153, 2019.
  - [20] F. Yang, L. Zhang, S. Yu, D. Prokhorov, X. Mei, and H. Ling, “Feature pyramid and hierarchical boosting network for pavement crack detection,” *IEEE Transactions on Intelligent Transportation Systems*, vol. 21, no. 4, pp. 1525–1535, 2019.
  - [21] Z. Al-Huda, B. Peng, M. A. Al-antari, R. N. A. Algburi, R. A. Saleh, and K. Moghalles, “Mdau-net: A multi-scale u-net with dual attention module for pavement crack segmentation,” in *2023 18th International Conference on Intelligent Systems and Knowledge Engineering (ISKE)*. IEEE, 2023, pp. 170–177.
  - [22] H. Huang, Y. Cai, C. Zhang, Y. Lu, A. Hammad, and L. Fan, “Crack detection of masonry structure based on thermal and visible image fusion and semantic segmentation,” *Automation in Construction*, vol. 158, p. 105213, 2024.
  - [23] J. Chen, Y. Lu, Q. Yu, X. Luo, E. Adeli, Y. Wang, L. Lu, A. L. Yuille, and Y. Zhou, “Transunet: Transformers make strong encoders for medical image segmentation,” *arXiv preprint arXiv:2102.04306*, 2021.
  - [24] H. Qi, X. Kong, Z. Jin, J. Zhang, and Z. Wang, “A vision-transformer-based convex variational network for bridge pavement defect segmentation,” *IEEE Transactions on Intelligent Transportation Systems*, 2024.
  - [25] Y. Feng, L. Jia, J. Zhang, and J. Chen, “Ffswinnet: Cnn-transformer combined network with fft for shale core sem image segmentation,” *IEEE Access*, 2024.
  - [26] A. G. Howard, M. Zhu, B. Chen, D. Kalenichenko, W. Wang, T. Weyand, M. Andreetto, and H. Adam, “Mobilenets: Efficient convolutional neural networks for mobile vision applications,” *arXiv preprint arXiv:1704.04861*, 2017.
  - [27] N. Ma, X. Zhang, H.-T. Zheng, and J. Sun, “Shufflenet v2: Practical guidelines for efficient cnn architecture

- design,” in *Proceedings of the European conference on computer vision (ECCV)*, 2018, pp. 116–131.
- [28] C. Li and C. Shi, “Constrained optimization based low-rank approximation of deep neural networks,” in *Proceedings of the European Conference on Computer Vision (ECCV)*, 2018, pp. 732–747.
- [29] S. Swaminathan, D. Garg, R. Kannan, and F. Andres, “Sparse low rank factorization for deep neural network compression,” *Neurocomputing*, vol. 398, pp. 185–196, 2020.
- [30] G. Zhu, J. Liu, Z. Fan, D. Yuan, P. Ma, M. Wang, W. Sheng, and K. C. Wang, “A lightweight encoder-decoder network for automatic pavement crack detection,” *Computer-Aided Civil and Infrastructure Engineering*, vol. 39, no. 12, pp. 1743–1765, 2024.
- [31] Y. Huang, Y. Liu, F. Liu, and W. Liu, “A lightweight feature attention fusion network for pavement crack segmentation,” *Computer-Aided Civil and Infrastructure Engineering*, 2024.
- [32] Q. Hou, L. Zhang, M.-M. Cheng, and J. Feng, “Strip pooling: Rethinking spatial pooling for scene parsing,” in *Proceedings of the IEEE/CVF conference on computer vision and pattern recognition*, 2020, pp. 4003–4012.
- [33] X. Zhu, W. Su, L. Lu, B. Li, X. Wang, and J. Dai, “Deformable detr: Deformable transformers for end-to-end object detection,” *arXiv preprint arXiv:2010.04159*, 2020.
- [34] J. Xu, Z. Xiong, and S. P. Bhattacharyya, “Pidnet: A real-time semantic segmentation network inspired by pid controllers,” in *Proceedings of the IEEE/CVF conference on computer vision and pattern recognition*, 2023, pp. 19 529–19 539.
- [35] Q. Li, X. Jia, J. Zhou, L. Shen, and J. Duan, “Rediscovering bce loss for uniform classification,” *arXiv preprint arXiv:2403.07289*, 2024.
- [36] C. H. Sudre, W. Li, T. Vercauteren, S. Ourselin, and M. Jorge Cardoso, “Generalised dice overlap as a deep learning loss function for highly unbalanced segmentations,” in *Deep Learning in Medical Image Analysis and Multimodal Learning for Clinical Decision Support: Third International Workshop, DLMIA 2017, and 7th International Workshop, ML-CDS 2017, Held in Conjunction with MICCAI 2017, Québec City, QC, Canada, September 14, Proceedings 3*. Springer, 2017, pp. 240–248.
- [37] M. Li, J. Yuan, Q. Ren, Q. Luo, J. Fu, and Z. Li, “Cnn-transformer hybrid network for concrete dam crack patrol inspection,” *Automation in Construction*, vol. 163, p. 105440, 2024.
- [38] Y. Shi, L. Cui, Z. Qi, F. Meng, and Z. Chen, “Automatic road crack detection using random structured forests,” *IEEE Transactions on Intelligent Transportation Systems*, vol. 17, no. 12, pp. 3434–3445, 2016.
- [39] M. Eisenbach, R. Stricker, D. Seichter, K. Amende, K. Debes, M. Sesselmann, D. Ebersbach, U. Stoeckert, and H.-M. Gross, “How to get pavement distress detection ready for deep learning? a systematic approach,” in *2017 international joint conference on neural networks (IJCNN)*. IEEE, 2017, pp. 2039–2047.
- [40] I. Katsamenis, E. Protopapadakis, N. Bakalos, A. Varvarigos, A. Doulamis, N. Doulamis, and A. Voulodimos, “A few-shot attention recurrent residual u-net for crack segmentation,” in *International Symposium on Visual Computing*. Springer, 2023, pp. 199–209.
- [41] Q. Zou, Y. Cao, Q. Li, Q. Mao, and S. Wang, “Crack-tree: Automatic crack detection from pavement images,” *Pattern Recognition Letters*, vol. 33, no. 3, pp. 227–238, 2012.
- [42] Z. Yao, J. Xu, S. Hou, and M. C. Chuah, “Cracknex: a few-shot low-light crack segmentation model based on retinex theory for uav inspections,” *arXiv preprint arXiv:2403.03063*, 2024.
- [43] F. Guo, Y. Qian, J. Liu, and H. Yu, “Pavement crack detection based on transformer network,” *Automation in Construction*, vol. 145, p. 104646, 2023.
- [44] S. Xie and Z. Tu, “Holistically-nested edge detection,” in *Proceedings of the IEEE international conference on computer vision*, 2015, pp. 1395–1403.
- [45] Z. Zhou, M. M. Rahman Siddiquee, N. Tajbakhsh, and J. Liang, “Unet++: A nested u-net architecture for medical image segmentation,” in *Deep Learning in Medical Image Analysis and Multimodal Learning for Clinical Decision Support: 4th International Workshop, DLMIA 2018, and 8th International Workshop, ML-CDS 2018, Held in Conjunction with MICCAI 2018, Granada, Spain, September 20, 2018, Proceedings 4*. Springer, 2018, pp. 3–11.
- [46] L.-C. Chen, Y. Zhu, G. Papandreou, F. Schroff, and H. Adam, “Encoder-decoder with atrous separable convolution for semantic image segmentation,” in *Proceedings of the European conference on computer vision (ECCV)*, 2018, pp. 801–818.
- [47] O. Oktay, J. Schlemper, L. L. Folgoc, M. Lee, M. Heinrich, K. Misawa, K. Mori, S. McDonagh, N. Y. Hammerla, B. Kainz *et al.*, “Attention u-net: Learning where to look for the pancreas,” *arXiv preprint arXiv:1804.03999*, 2018.
- [48] Y. Liu, M.-M. Cheng, X. Hu, K. Wang, and X. Bai, “Richer convolutional features for edge detection,” in *Proceedings of the IEEE conference on computer vision and pattern recognition*, 2017, pp. 3000–3009.
- [49] M. Pu, Y. Huang, Q. Guan, and H. Ling, “Rindnet: Edge detection for discontinuity in reflectance, illumination, normal and depth,” in *Proceedings of the IEEE/CVF international conference on computer vision*, 2021, pp. 6879–6888.